

Enhanced Li-ion Dynamics in Trivalently Doped Lithium Phosphidosilicate Li_2SiP_2 : A Candidate Material as a Solid Li Electrolyte - Supporting Information

Stephen R. Yeandel,[†] David O. Scanlon,[‡] and Pooja Goddard^{*,†}

[†]*Department of Chemistry, Loughborough University, Loughborough, LE11 3TU*

[‡]*Department of Chemistry, University College London, 20 Gordon Street, London WC1H
0AJ, UK.*

E-mail: P.Goddard@lboro.ac.uk

DFT parameters

Program: VASP¹

Structure: Li₂SiP₂²

Basis Set: PAW Pseudopotentials³ and Planewaves

Functional: PBEsol⁴

ISPIN: 2 (spin polarised)

Energy Cutoff: 1000 eV

AIMD SMASS setting: 20.0

Simulation cells

Table S1: LSP simulation cells, all angles 90°

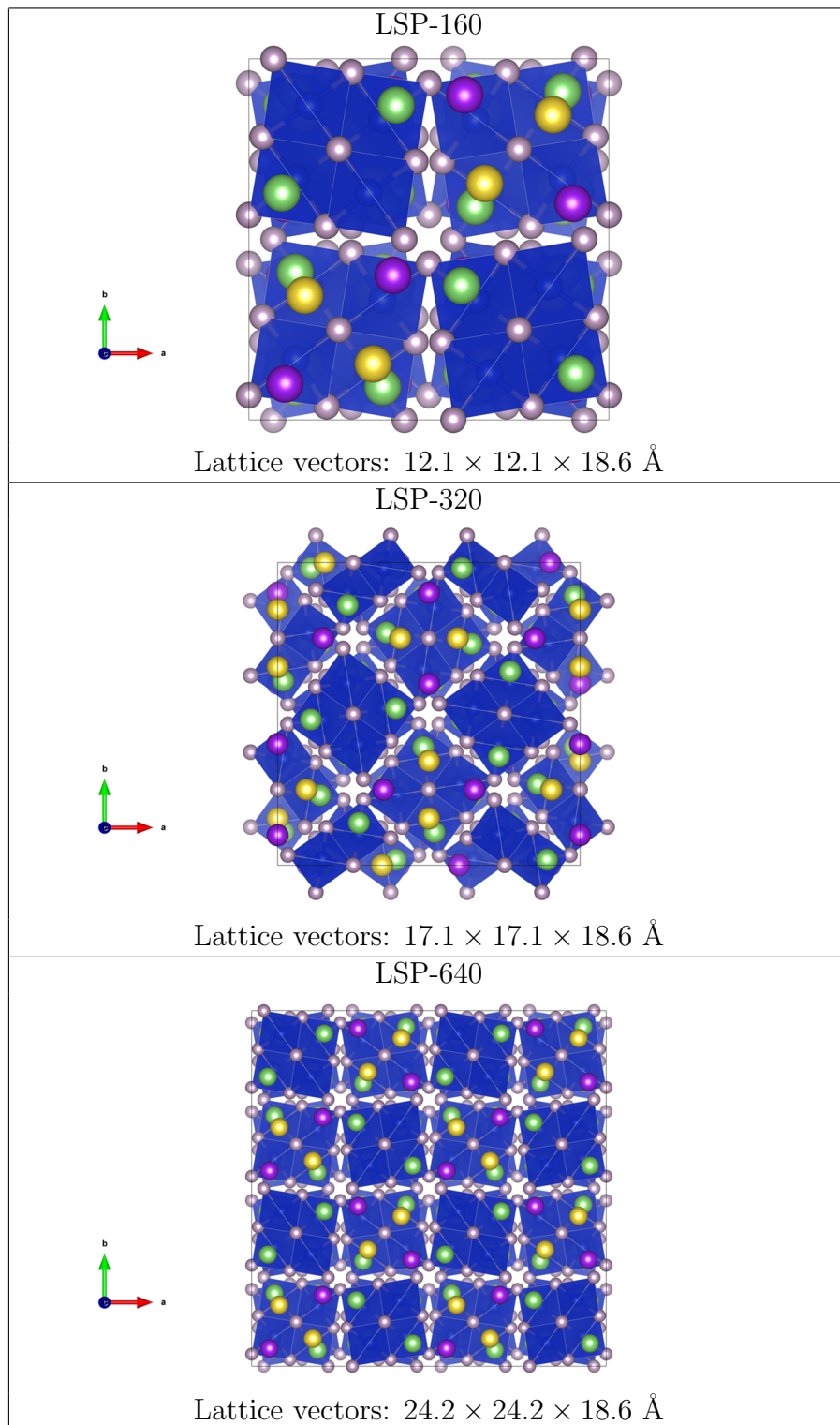


Table S2: Comparison of experimental and calculated lattice parameters

Observable	Toffoletti et al. ⁵	Haffner et al. ²	Calculated (LSP-160)
a (Å)	12.11	12.11	12.09
b (Å)	12.11	12.11	12.09
c (Å)	18.63	18.68	18.56
α (°)	90.00	90.00	90.00
β (°)	90.00	90.00	90.00
γ (°)	90.00	90.00	90.00

The LSP-160 simulation cell corresponds to the reported unit cell and is the smallest orthorhombic cell of the LSP structure. The LSP-320 system is generated as a $\sqrt{2} \times \sqrt{2} \times 1$ expansion of the LSP-160 simulation cell. The LSP-640 cell is a $2 \times 2 \times 1$ expansion of the LSP-160 simulation cell. The k-point grids for each simulation cell were tested for convergence and are given in Table S3.

Table S3: K-point grids used for various simulation cell sizes

Material	Atoms	k-point grid
Li ₂ SiP ₂	160	$3 \times 3 \times 2$
Li ₂ SiP ₂	320	$2 \times 2 \times 2$
Li ₂ SiP ₂	640	$1 \times 1 \times 2$
Li ₃ P	8	$12 \times 12 \times 12$
BP	8	$7 \times 7 \times 7$
AlP	8	$7 \times 7 \times 7$
GaP	8	$7 \times 7 \times 7$

Lithium vacancy energy

Table S4: Lithium cation point vacancy energies in a LSP-160 cell (total charge -1 on remaining lattice)

Site	Relative Energy (eV)
1	0.086
2	0.063
3	0.000

Defect energy calculation

The raw energies reported here were used to compute the defect energies in Table 2 using Equations 5 and 6 and are included for completeness.

Table S5: Bulk material energies

Material	Energy (eV/pfu)
Li ₂ SiP ₂	-23.914
Li ₃ P	-14.442
BP	-13.677
AlP	-10.997
GaP	-9.865

Table S6: Raw defective simulation cell energies

Defect	Simulation cell	Formula	Energy (eV)
$B'_{Si} + Li_i^\bullet$	LSP-160	$Li_{65}Si_{31}B_1P_{64}$	-768.254
$B'_{Si} + Li_i^\bullet$	LSP-320	$Li_{129}Si_{63}B_1P_{128}$	-1533.494
$B'_{Si} + Li_i^\bullet$	LSP-640	$Li_{257}Si_{127}B_1P_{256}$	-3064.011
$Al'_{Si} + Li_i^\bullet$	LSP-160	$Li_{65}Si_{31}Al_1P_{64}$	-766.739
$Al'_{Si} + Li_i^\bullet$	LSP-320	$Li_{129}Si_{63}Al_1P_{128}$	-1531.991
$Al'_{Si} + Li_i^\bullet$	LSP-640	$Li_{257}Si_{127}Al_1P_{256}$	-3062.505
$Ga'_{Si} + Li_i^\bullet$	LSP-160	$Li_{65}Si_{31}Ga_1P_{64}$	-765.477
$Ga'_{Si} + Li_i^\bullet$	LSP-320	$Li_{129}Si_{63}Ga_1P_{128}$	-1530.728
$Ga'_{Si} + Li_i^\bullet$	LSP-640	$Li_{257}Si_{127}Ga_1P_{256}$	-3061.242
$B_{Li}^{\bullet\bullet} (Li\ site\ 1) + 2V'_{Li}$	LSP-160	$Li_{61}B_1Si_{32}P_{64}$	-760.185
$B_{Li}^{\bullet\bullet} (Li\ site\ 2) + 2V'_{Li}$	LSP-160	$Li_{61}B_1Si_{32}P_{64}$	-760.180
$B_{Li}^{\bullet\bullet} (Li\ site\ 3) + 2V'_{Li}$	LSP-160	$Li_{61}B_1Si_{32}P_{64}$	-760.894
$B_{Li}^{\bullet\bullet} (Li\ site\ 1) + 2V'_{Li}$	LSP-320	$Li_{125}B_1Si_{64}P_{128}$	-1525.388
$B_{Li}^{\bullet\bullet} (Li\ site\ 2) + 2V'_{Li}$	LSP-320	$Li_{125}B_1Si_{64}P_{128}$	-1526.036
$B_{Li}^{\bullet\bullet} (Li\ site\ 3) + 2V'_{Li}$	LSP-320	$Li_{125}B_1Si_{64}P_{128}$	-1526.076
$B_{Li}^{\bullet\bullet} (Li\ site\ 1) + 2V'_{Li}$	LSP-640	$Li_{253}B_1Si_{128}P_{256}$	-3055.913
$B_{Li}^{\bullet\bullet} (Li\ site\ 2) + 2V'_{Li}$	LSP-640	$Li_{253}B_1Si_{128}P_{256}$	-3056.521
$B_{Li}^{\bullet\bullet} (Li\ site\ 3) + 2V'_{Li}$	LSP-640	$Li_{253}B_1Si_{128}P_{256}$	-3056.587
$Al_{Li}^{\bullet\bullet} (Li\ site\ 1) + 2V'_{Li}$	LSP-160	$Li_{61}Al_1Si_{32}P_{64}$	-759.865
$Al_{Li}^{\bullet\bullet} (Li\ site\ 2) + 2V'_{Li}$	LSP-160	$Li_{61}Al_1Si_{32}P_{64}$	-759.836
$Al_{Li}^{\bullet\bullet} (Li\ site\ 3) + 2V'_{Li}$	LSP-160	$Li_{61}Al_1Si_{32}P_{64}$	-759.300
$Al_{Li}^{\bullet\bullet} (Li\ site\ 1) + 2V'_{Li}$	LSP-320	$Li_{125}Al_1Si_{64}P_{128}$	-1525.097
$Al_{Li}^{\bullet\bullet} (Li\ site\ 2) + 2V'_{Li}$	LSP-320	$Li_{125}Al_1Si_{64}P_{128}$	-1525.101
$Al_{Li}^{\bullet\bullet} (Li\ site\ 3) + 2V'_{Li}$	LSP-320	$Li_{125}Al_1Si_{64}P_{128}$	-1524.543
$Al_{Li}^{\bullet\bullet} (Li\ site\ 1) + 2V'_{Li}$	LSP-640	$Li_{253}Al_1Si_{128}P_{256}$	-3055.624
$Al_{Li}^{\bullet\bullet} (Li\ site\ 2) + 2V'_{Li}$	LSP-640	$Li_{253}Al_1Si_{128}P_{256}$	-3055.616
$Al_{Li}^{\bullet\bullet} (Li\ site\ 3) + 2V'_{Li}$	LSP-640	$Li_{253}Al_1Si_{128}P_{256}$	-3055.078
$Ga_{Li}^{\bullet\bullet} (Li\ site\ 1) + 2V'_{Li}$	LSP-160	$Li_{61}Ga_1Si_{32}P_{64}$	-758.605
$Ga_{Li}^{\bullet\bullet} (Li\ site\ 2) + 2V'_{Li}$	LSP-160	$Li_{61}Ga_1Si_{32}P_{64}$	-758.596
$Ga_{Li}^{\bullet\bullet} (Li\ site\ 3) + 2V'_{Li}$	LSP-160	$Li_{61}Ga_1Si_{32}P_{64}$	-758.102
$Ga_{Li}^{\bullet\bullet} (Li\ site\ 1) + 2V'_{Li}$	LSP-320	$Li_{125}Ga_1Si_{64}P_{128}$	-1523.838
$Ga_{Li}^{\bullet\bullet} (Li\ site\ 2) + 2V'_{Li}$	LSP-320	$Li_{125}Ga_1Si_{64}P_{128}$	-1523.862
$Ga_{Li}^{\bullet\bullet} (Li\ site\ 3) + 2V'_{Li}$	LSP-320	$Li_{125}Ga_1Si_{64}P_{128}$	-1523.355
$Ga_{Li}^{\bullet\bullet} (Li\ site\ 1) + 2V'_{Li}$	LSP-640	$Li_{253}Ga_1Si_{128}P_{256}$	-3054.367
$Ga_{Li}^{\bullet\bullet} (Li\ site\ 2) + 2V'_{Li}$	LSP-640	$Li_{253}Ga_1Si_{128}P_{256}$	-3054.378
$Ga_{Li}^{\bullet\bullet} (Li\ site\ 3) + 2V'_{Li}$	LSP-640	$Li_{253}Ga_1Si_{128}P_{256}$	-3053.888

Final defect energies were calculated by taking the raw energies above and using Equations 5 and 6. We again note that as defect and compensating defect are in the same simulation cell there is a contribution due to clustering included.

The defect energies for Equation 5 were computed via:

$$E_{\text{Si-defect-160}} = E[\text{Li}_{65}\text{Si}_{31}\text{M}_1\text{P}_{64}] - 31 E[\text{Li}_2\text{SiP}_2] - E[\text{MP}] - E[\text{Li}_3\text{P}] \quad (\text{S1})$$

$$E_{\text{Si-defect-320}} = E[\text{Li}_{129}\text{Si}_{63}\text{M}_1\text{P}_{128}] - 63 E[\text{Li}_2\text{SiP}_2] - E[\text{MP}] - E[\text{Li}_3\text{P}] \quad (\text{S2})$$

$$E_{\text{Si-defect-640}} = E[\text{Li}_{257}\text{Si}_{127}\text{M}_1\text{P}_{256}] - 127 E[\text{Li}_2\text{SiP}_2] - E[\text{MP}] - E[\text{Li}_3\text{P}] \quad (\text{S3})$$

The defect energies for Equation 6 were computed via:

$$E_{\text{Li-defect-160}} = E[\text{Li}_{61}\text{M}_1\text{Si}_{32}\text{P}_{64}] + E[\text{Li}_3\text{P}] - 32 E[\text{Li}_2\text{SiP}_2] - E[\text{MP}] \quad (\text{S4})$$

$$E_{\text{Li-defect-320}} = E[\text{Li}_{125}\text{M}_1\text{Si}_{64}\text{P}_{128}] + E[\text{Li}_3\text{P}] - 64 E[\text{Li}_2\text{SiP}_2] - E[\text{MP}] \quad (\text{S5})$$

$$E_{\text{Li-defect-640}} = E[\text{Li}_{253}\text{M}_1\text{Si}_{128}\text{P}_{256}] + E[\text{Li}_3\text{P}] - 128 E[\text{Li}_2\text{SiP}_2] - E[\text{MP}] \quad (\text{S6})$$

AIMD volume equilibration

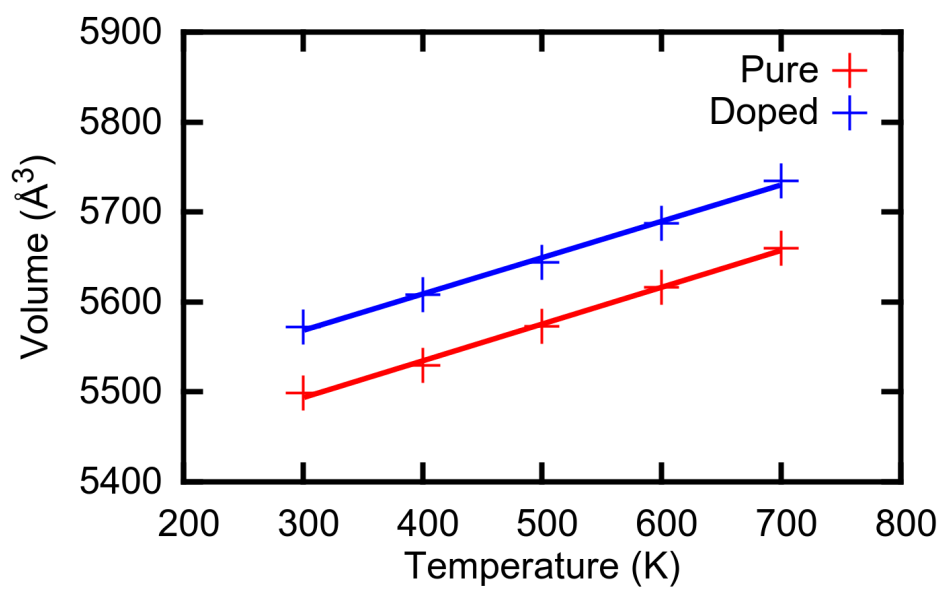
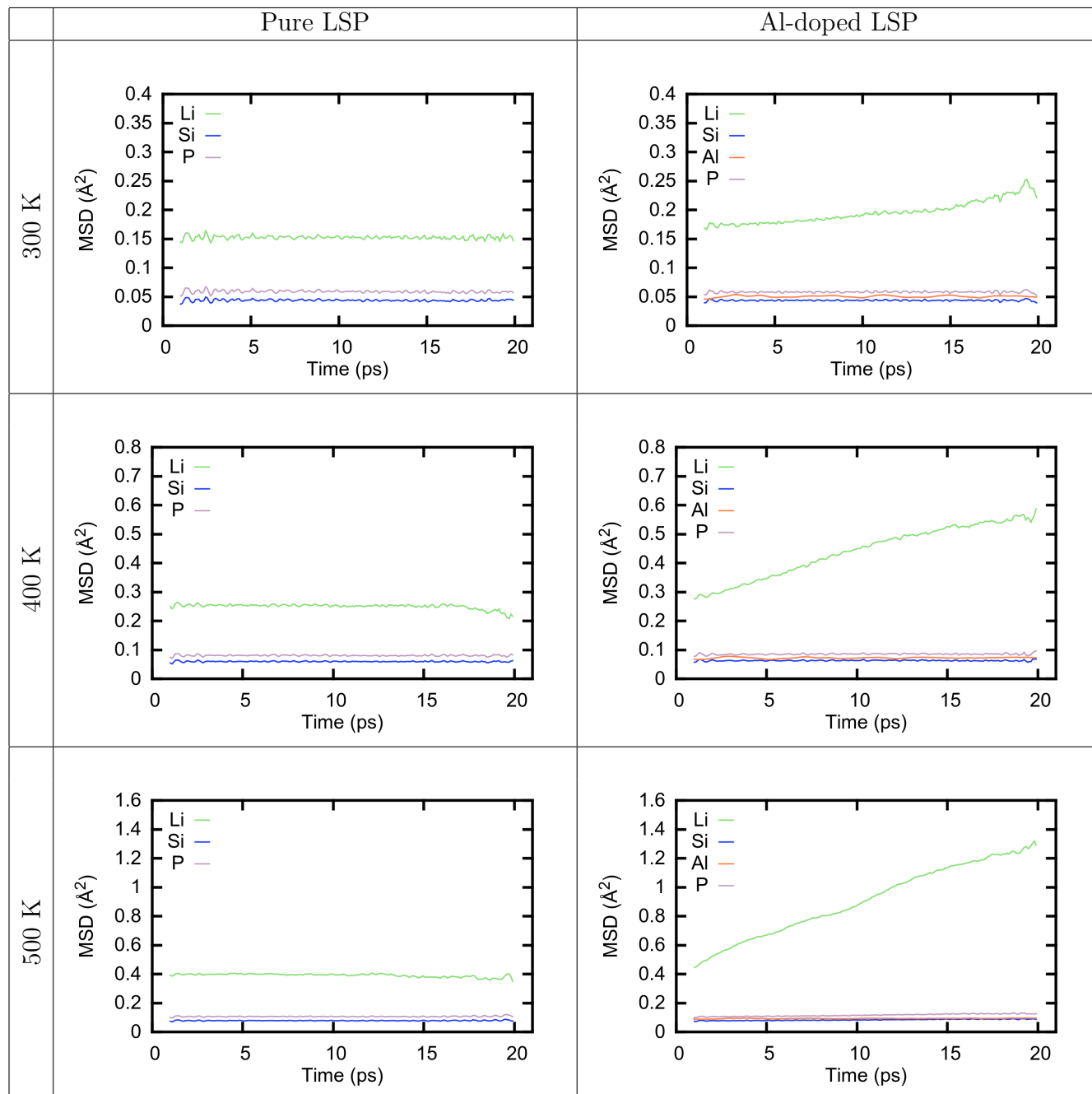
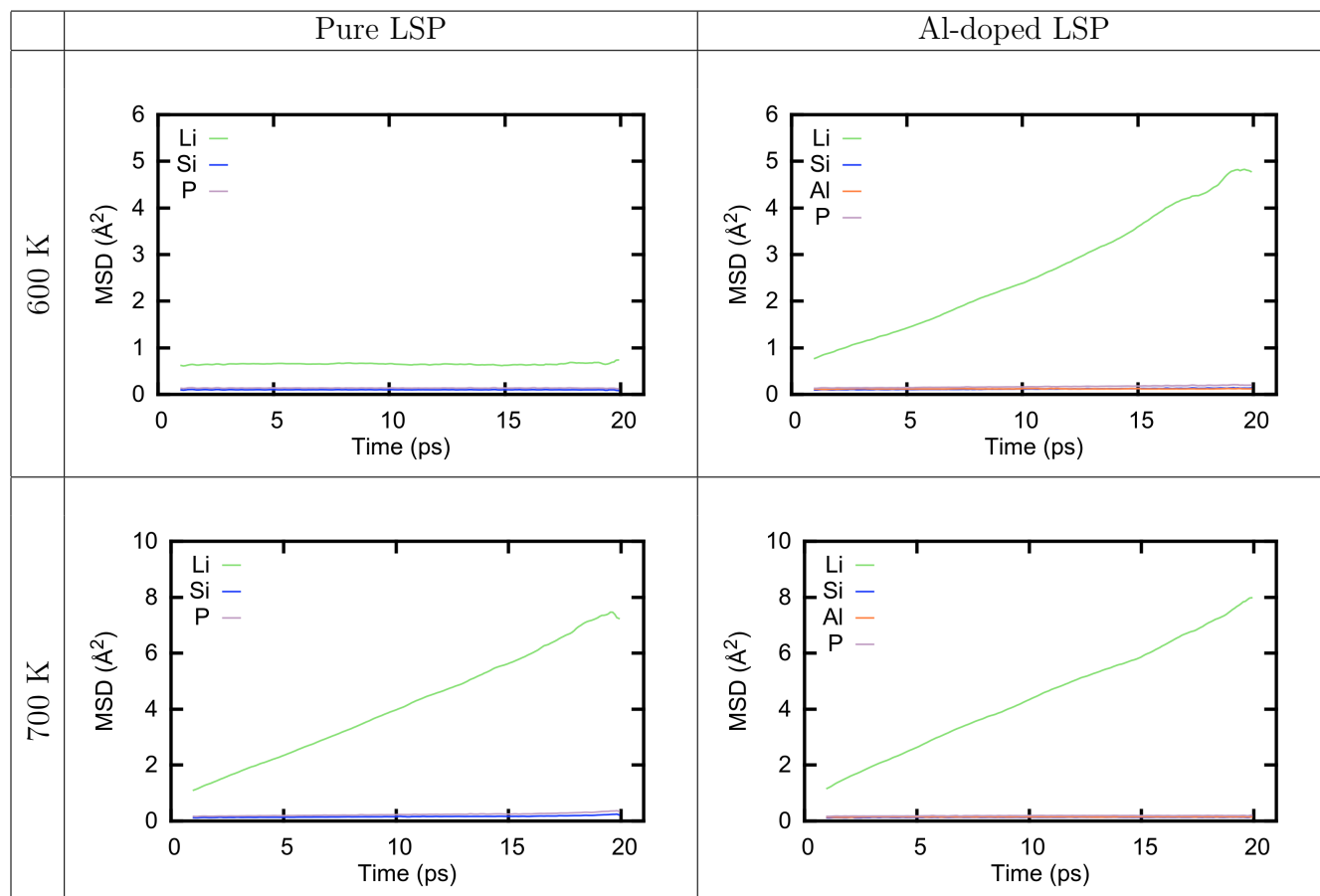


Figure S1: Average cell volume of pure and Al'_{Si} doped LSP after Langevin MD.

MSDs

Table S7: Average MSD of pure and Al doped LSP (including all ions) showing that only lithium ions are diffusing.





NEB calculations

Li site 2 pathway

To determine why the site-2 pathway shows such good lithium mobility, Nudged Elastic Band (NEB) calculations were performed.^{6,7} Three mechanisms using the site 2 pathway were studied with NEB, interstitial, vacancy and stoichiometric. The interstitial type mechanism, observed in MD, involves additional ions on originally unoccupied sites which can then either move around occupied sites, or alternatively displace ions from occupied sites and thereby generate a new interstitial ion. The vacancy type mechanism involves the hopping of ions from an occupied site to an unoccupied site, and may also be considered as the diffusion of V'_{Li} species. The stoichiometric type mechanism involves the simultaneous movement of multiple ions such that there is no lasting defect state.

The NEB calculations were performed by selecting a start and end image and performing a linear interpolation to produce 10 images which were then allowed to relax, with a fictitious spring linking adjacent images.^{6,7} The LSP-160 supercell was used for all NEB calculations. The electronic structure was optimised using a reduced k-point grid, involving only the Γ -point, for reasons of computational time. The 1000 eV plane wave energy cut-off was retained from previous calculations. Once again a force tolerance of $1.0 \times 10^{-2} \text{ eV}\cdot\text{\AA}^{-1}$ was applied for convergence.

To generate a stoichiometric hop it is sufficient to displace all lithium ions one step to the adjacent site, resulting in a single hopping mechanism, which we term hop s1. The average hop distance of hop s1 is 3.60 \AA . When a vacancy diffusion mechanism is considered there are two hopping steps, we have termed these hop v1 and hop v2. Hop v1 is shorter at 3.32 \AA and hop v2 requires a displacement of 3.87 \AA .

The interstitial mechanism is harder to quantify as the insertion of an interstitial results in a fairly even distribution of lithium ions within the site 2 to site 2 pathway and it is unclear how far the defect will move in a single hop. To solve this problem we generated a

single initial interstitial NEB pathway which returns to the original state within symmetry at the end of the NEB pathway. From this initial interstitial NEB pathway local energy minima could be identified and these were minimised to find that in total there are two main hopping steps for the interstitial mechanism, we have termed these hop i1 and hop i2. Hop i1 has an average hopping distance of 2.17 Å whereas hop i2 has an average hopping distance of 0.89 Å and may be considered more as a rearrangement of lithium ions which allows a further hop i1 to occur.

In addition to the individual hops identified, we also considered concerted mechanisms which involve vacancy or interstitial defects moving multiple sites in a single hop. These concerted mechanisms always resulted in higher migration barriers or minimised in to two distinct hops during the NEB calculations. The relative energies of the potential site 2 mechanisms are plotted in Figure S2.

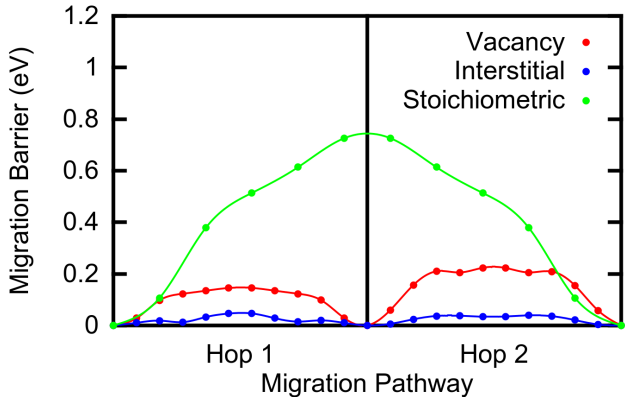


Figure S2: Energy barriers calculated via the NEB for potential hopping mechanisms in the site 2 pathway of LSP. The Stoichiometric mechanism only has one hopping mechanism but has been extended for clarity

It is clear from Figure S2 that the lithium interstitial pathway has the lowest activation energy, requiring only 0.05 eV to activate both hop i1 and hop i2. In comparison, the vacancy and stoichiometric pathways require activation energies of 0.2 eV and 0.8 eV respectively. The very low energy barriers to migration found in hops i1 and i2 originate from the relatively small displacement of other ions in the system during migration.

The very low energy barrier to lithium migration in the interstitial site 2 pathway in-

dicating it may be used significantly when lithium interstitial ions are present. Therefore, the increased diffusion coefficients seen in the Al'_{Si} doped systems likely originate from the priming with multiple Li'_{i} defects.

Li vacancy pathways

The vacancy component of the lithium diffusion pathways was observed to follow a much more complex path. Whilst it is difficult to study interstitial pathways without preceding data indicating the initial and final location of interstitial defects, vacancy mechanisms are much easier to identify and study. Thus, to identify the likely pathway of the vacancy component of the lithium Frenkel pair, several lithium vacancy diffusion mechanisms were studied with NEB using the same approach as before. All of the identified vacancy diffusion mechanisms showed activation energies on a par with those observed for the site 2 to site 2 vacancy pathway, Figure S3.

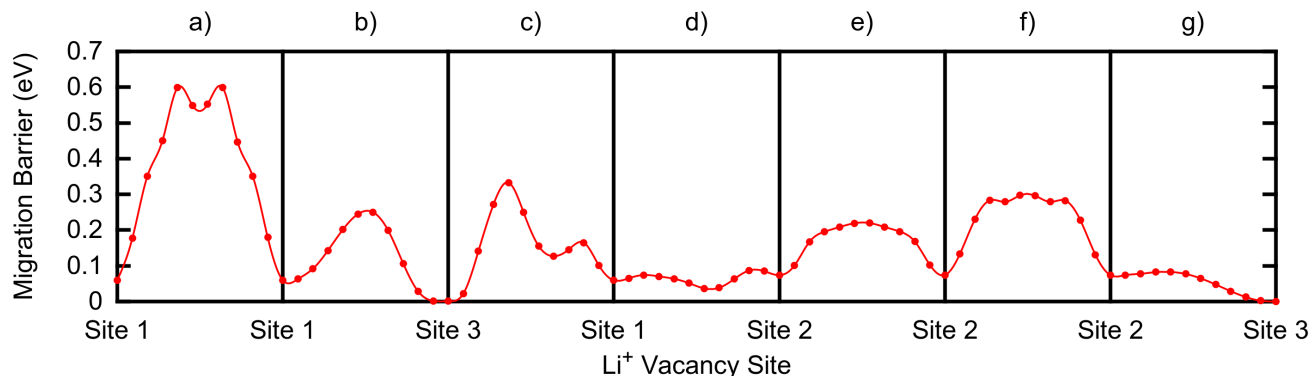


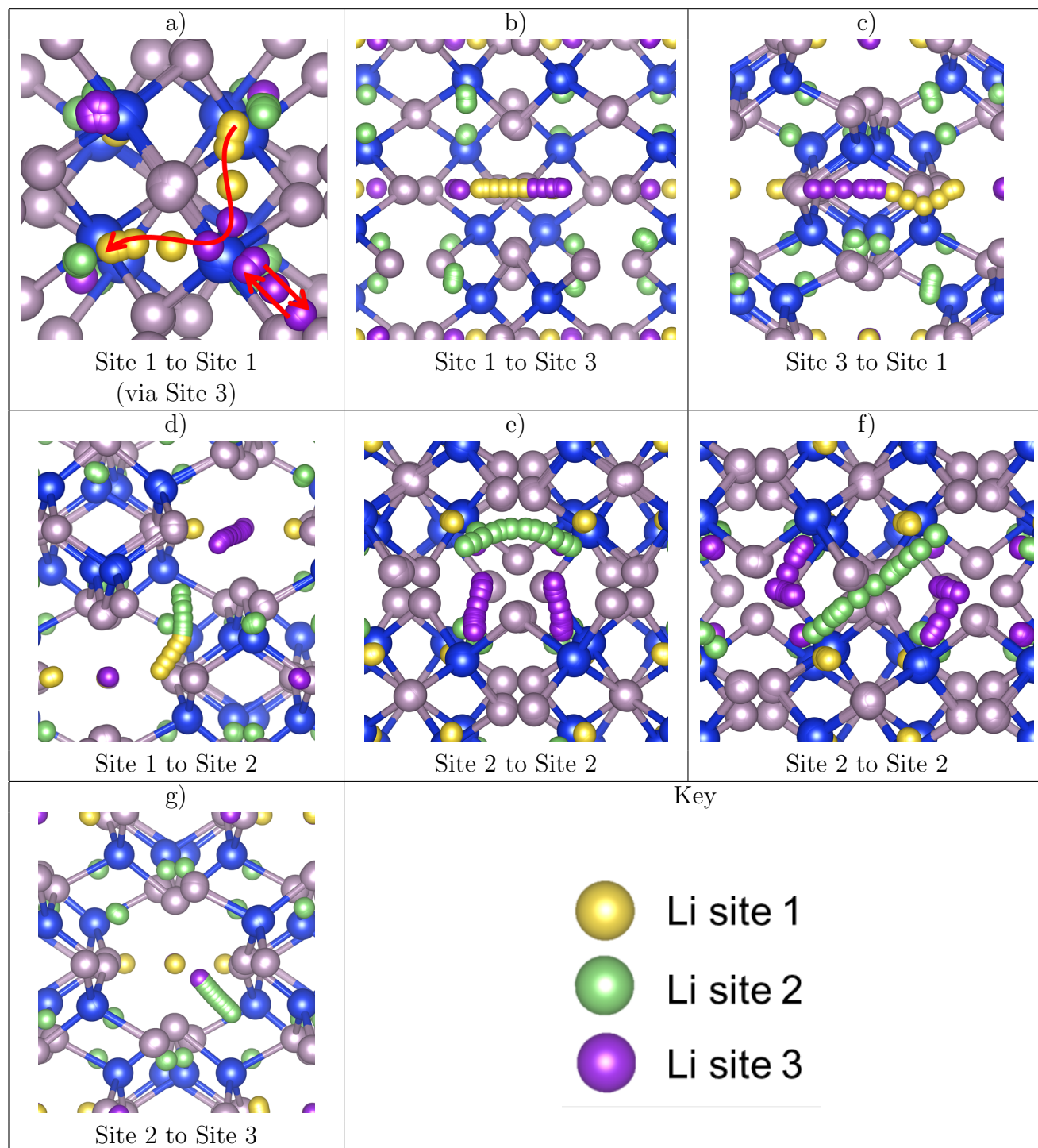
Figure S3: Lithium vacancy migration barriers in Li_2SiP_2 normalised to the lowest energy lithium vacancy on lithium site-3. Site labels correspond to position of Li vacancy defect. For corresponding pathways please see Table S8

The activation energies obtained from the vacancy NEB calculations, Figure S3, are generally within agreement with the activation energies as obtained from AIMD of 0.24 to 0.3 eV. Interestingly, there are two mechanisms with small migration barriers which will allow a Li^+ vacancy to move away from site 2. The first barrier is on the order of 0.02 eV

and involves movement of the Li^+ vacancy from site 2 to a site between site 1 and site 2 and then on to site 1. The second barrier is on the order of 0.01 eV and involves movement of the Li^+ vacancy from site 2 to site 3. These low energy pathways for migration of Li^+ vacancies away from the site 2 pathway further support the generation and separation of the Frenkel pair as observed in AIMD.

Of note is that the two low energy barrier vacancy mechanisms together form a double helix pathway through the material in the z direction, with an overall low activation energy of approximately 0.1 eV. This suggests that whereas the interstitial mechanism may be dominant in the x-y plane due to the low energy site 2 interstitial pathway, the vacancy mechanisms may dominate the overall diffusion of the system by utilising the helical pathway and other relatively low energy vacancy diffusion pathways present. Thus, while trivalent doping in Li_2SiP_2 may act to boost the interstitial x-y plane diffusion mechanism (via site 2), the vacancy mechanism in the z direction may be reduced.

Table S8: NEB vacancy pathways in Li_2SiP_2 . Note that hop labels are for lithium vacancies, whereas atomic positions are displayed. For corresponding energy barriers please see Figure S3



Calculated electronic properties

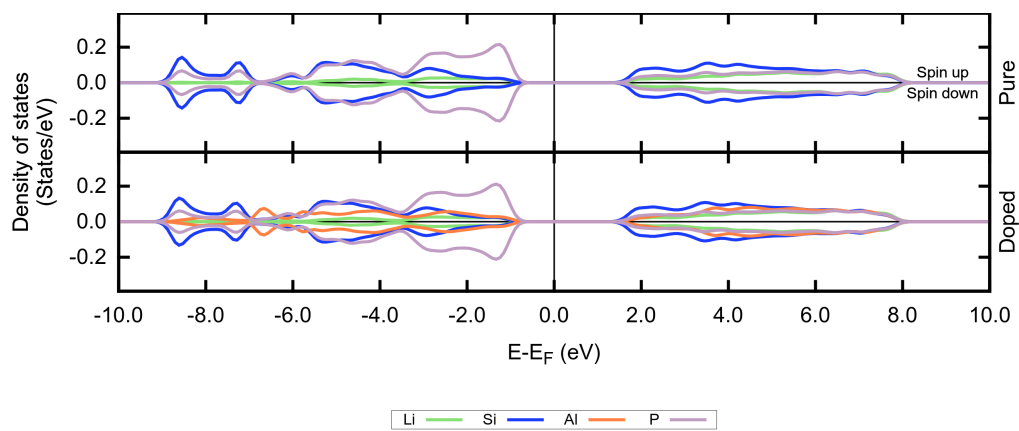


Figure S4: Electronic DOS for pure LSP and LSP doped with a single Al substitution and Li interstitial.

References

- (1) Kresse, G.; Hafner, J. *Physical Review B* **1994**, *49*, 14251.
- (2) Haffner, A.; Bräuniger, T.; Johrendt, D. *Angewandte Chemie International Edition* **2016**, *55*, 13585–13588.
- (3) Blöchl, P. E. *Physical review B* **1994**, *50*, 17953.
- (4) Perdew, J. P.; Ruzsinszky, A.; Csonka, G. I.; Vydrov, O. A.; Scuseria, G. E.; Constantin, L. A.; Zhou, X.; Burke, K. *Physical Review Letters* **2008**, *100*, 136406.
- (5) Toffoletti, L.; Kirchhain, H.; Landesfeind, J.; Klein, W.; van Wüllen, L.; Gasteiger, H. A.; Fässler, T. F. *Chemistry-A European Journal* **2016**, *22*, 17635–17645.
- (6) Mills, G.; Jónsson, H.; Schenter, G. K. *Surface Science* **1995**, *324*, 305–337.
- (7) Jónsson, H.; Mills, G.; Jacobsen, K. W. *Classical and quantum dynamics in condensed phase simulations*; World Scientific, 1998; pp 385–404.